JOURNAL OF MATERIALS SCIENCE **37** (2002) 3497 – 3507

Finite element analysis of a polymer composite subjected to a sliding steel asperity

Part II: *Parallel and anti-parallel fibre orientations*

K. FRIEDRICH
Institute for Composite Materials Ltd. (IVW), University of Kaiserslautern, D-67663 Kaiserslautern, Erwin-Schrödinger Str. Geb. 58, Germany
E-mail: friedric@ivw.uni-kl.de

K. VÁRADI, T. GODA
Institute of Machine Design, Budapest University of Technology and Economics, H-1111 Budapest, Müegyetem rkp. 3., Hungary
E-mail: varadik@eik.bme.hu

H. GIERTZSCH
Institute for Composite Materials Ltd. (IVW), University of Kaiserslautern, D-67663 Kaiserslautern, Erwin-Schrödinger Str. Geb. 58, Germany

Finite element (FE) micro-models have been developed in order to determine contact, stress and strain conditions produced by a steel asperity sliding on the surface of a fibre-reinforced polymer composite. Two cases were studied, i.e. a parallel and an anti-parallel fibre orientation relative to the sliding direction. In order to get more realistic simulation results relating to the failure conditions in the composite structure, FE contact macro/micro-models were used, contrary to the so far widely applied anisotropic analytical or numerical macro-models. To model a "micro-environment" as part of a "macro-environment", the displacement coupling technique was introduced. The contact analysis operates on both the macro- and the micro-level, applying node-to-node contact elements. The contact results, especially the contact pressure distribution, can characterize the real fibre/matrix micro-system. Displacement and strain results lead to explanations of fibre related phenomena, matrix shear effects, and fibre/matrix debonding events. On the basis of the stress results, conclusions were drawn on the possible wear mechanisms of the fibre-reinforced polymer composite. For parallel fibre orientation, fibre/matrix debonding as a result of shear stresses at the interface, matrix shear type failure and fibre thinning are the dominant sliding wear mechanisms. If an anti-parallel fibre orientation is considered, matrix shear, tension/compression type fibre/matrix debonding and fibre thinning, associated with fibre cracking events, are the most dominant wear mechanisms. To study the wear mechanisms experimentally, diamond tip scratch tests were carried out, showing that the predicted failure events occur also in reality.

1. Introduction

Polymer composites are being used more and more as structural components that are very often subjected to friction and wear loading. In certain situations, the coefficient of friction is of the highest importance, but largely it is the mechanical load carrying capacity and the wear life of components that determine their acceptability in industrial applications. Depending on the particular practical application the kind of wear loading can be very different, and therefore the structure of the composite material used for these applications can also be very different in order to fulfill the particular requirements [1].

Sliding wear of polymeric composites against a smooth steel surface was investigated by Voss and Friedrich [2] for the case of short-fibre-reinforced PEEK composites. They studied the wear mechanisms for sliding and abrasive wear cases. They proposed that "thinning of the fibers by the sliding steel surface, fibre breakage and subsequent removal together with pulverization of the fibers are the main fibre related wear mechanisms". They found that four different mechanisms dominate the process of material removal: matrix wear, fibre sliding wear, fibre cracking and wear by fibre/matrix separation (debonding) at the interface. These four dominant phenomena occur in the immediate surface region, which are one to two fibre diameters beneath the surface. On the basis of their and further observations, Fig. 1 reviews the typical wear mechanisms in the cases of parallel (P) and anti-parallel (AP) fibre orientations.

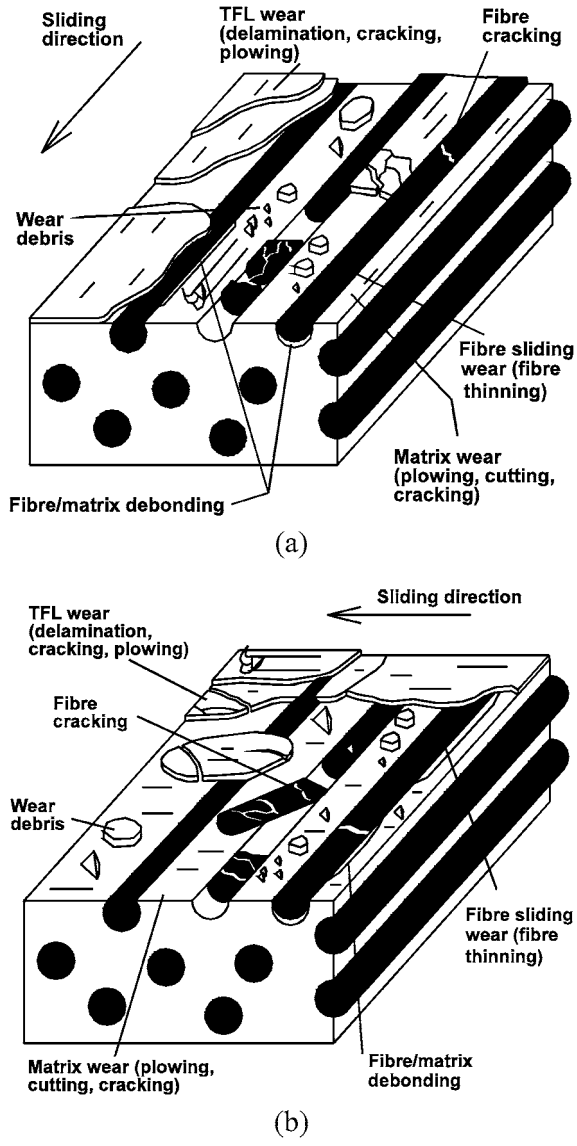

Figure 1 Typical wear mechanisms of fibre-reinforced polymer composites; P-fibre orientation (a) and AP-fibre orientation (b) (TFL means transfer film layer or layer of compacted wear debris).

The friction behavior of these materials has been intensively studied in the last couple of years, in order to improve their tribological performance. In particular, several efforts were undertaken to better understand the wear processes of composites against steel counterparts. As the contact, stress and deformation characteristics during sliding contact have a considerable impact on the wear of structural elements, it is essential to evaluate them in more detail. These evaluations traditionally followed a macroscopic approach, assuming homogeneous, anisotropic material properties as derived by rule of mixture type relationships [3]. A disadvantage of this macroscopic approach is that it is not suitable for modelling the actual interaction of the fibers and matrix of the composite with the asperities of the counterpart.

In [4], Ovaert analyzed P-fibre orientation (relative to the sliding direction) by using anisotropic half-space models. The individual fibre was modelled as an infinite beam on an elastic foundation, with the foundation stiffness approximated from the results of the contact simulation. From these results, a fibre stress due to deformation and sliding is estimated. The normal and tangential forces from the rough surface will induce tensile stresses in the fibers at the surface, which are a function of the counterface asperity geometry and the asperity load. These tensile stresses play an important role in the deterioration of the surface fibers, which leads to subsequent fibre-matrix separation and enhanced wear. Later Ovaert [5] extended this model to AP-fibre orientation. According to his conclusion, a rough correlation exists between normalized wear rates and calculated stress—deformation parameters for several polymer composites.

A FE micro-model was used in [6] to determine contact and stress states produced by a steel ball pressed into a fibre-reinforced composite. Location and distribution of sub-surface stresses and strains were studied for N- as well as P-fibre orientation. It was established that in the case of N-fibre orientation there is a high shear stress region below the surface, from where the fibre/matrix interfacial failure initiates before propagating to the surface. In the case of P-fibre orientation, the matrix is subjected to both shear and compression type straining, yielding and local plastic deformation, while the characteristic deformations of the fibers are bending and compression.

The present study aims at the development of FE micro-models that allow to provide explanations for different failure mechanisms based on the evaluation of contact, stress and strain conditions produced by a sliding hemispheric asperity (Fig. 2). In particular, it is expected that this approach will give answers about the actual fibre stresses, matrix strains, events of fibre/matrix debonding etc. The latter features will finally lead to the characteristic wear mechanisms of fibre-reinforced polymer composites, as shown in Fig. 1.

The FE macro- and micro-models were created and solved by the contact and static modules of the COSMOS/M system [7].

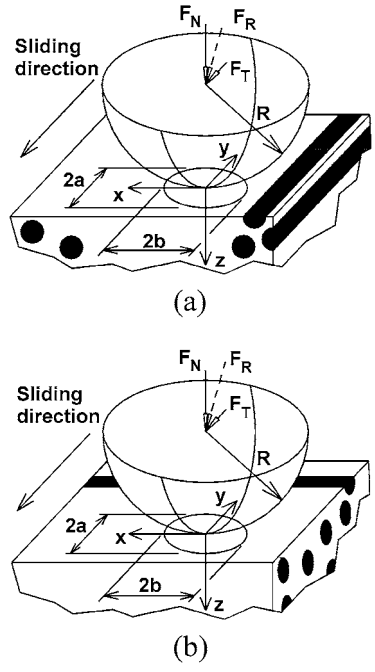

Figure 2 The modelled sliding asperity with normal and tangential loading; P-fibre orientation (a) and AP-fibre orientation (b).

TABLE I Mechanical properties of the materials (σ_Y is the yield strength)

$V_f = 0.61$	Steel [9]	CF [10]	PEEK [10]	Composite
E_{11}(MPa)		235000		144921
E_{22}(MPa)	210000	15000	4030	7276
E_{33}(MPa)		15000		7276
G_{12}(MPa)		6432		2734
G_{13}(MPa)	80769	6432	1439	2734
G_{23}(MPa)		5357		2419
υ_{12}		0.166		0.257
υ_{13}	0.3	0.166	0.4	0.257
υ_{23}		0.4		0.504
σ_Y(MPa)	3000	–	137	–

2. Experimental details

The composite material studied here is a CF (carbon fibre) reinforced PEEK (polyether-etherketone) with a fibre volume fraction of 0.61 [8]. Its mechanical properties along with those of the steel asperity are listed in Table I [9, 10]. The principal material directions, indicated by 1, 2 and 3 in Table I are shown in Fig. 2 for the cases studied. The anisotropic composite material properties were specified using the equations listed in the Appendix.

The radius of the steel asperity, modelled by a hemisphere, is $R = 0.45$ mm. The normal load is $F_N = 1$ N, and the friction coefficients are $\mu = 0.28$ (P) and $\mu = 0.3$ (AP), according to previous experimental studies [11]. In the models, a larger radius was required than that of the real average asperity (some ten microns) in order to be able to compare our results with experimental test results.

The experimental verification of the wear mechanisms, expected from the modelling studies, was attempted by single scratch tests, carried out with various scratch tips. A steel ball with the given diameter of 0.9 mm as well as a diamond Rockwell test indentor with a tip angle of 120° and a tip radius of 100 μm were compressed onto the composite specimen and slowly slid. The normal loads on the indentor varied between 1 and 3 N. Scanning electron microscopy was used to analyze the individual features which occurred in the scratch grooves.

3. FE macro and micro contact models

To evaluate the stresses in a fibre/matrix micro-system, a FE micro-model was created. This micro-model is "built into" a larger (homogeneous and anisotropic) macro-model to represent a larger segment of the original body, in order to achieve a higher accuracy. The displacement coupling technique and the FE macro-models are presented and described in [12].

On the composite sides of the FE micro contact models for P and AP fibre orientations, the fiber diameter is 8 μm, and the volume fraction is 0.61. The characteristic data of the micro-models are collected in Table II.

TABLE III Contact parameters for normal and frictional contact problems in the case of P-fibre orientation

Case no.		μ	δ (μm)	$2a$ (μm)	$2b$ (μm)	$p_{\max}$ (MPa)
1	FE macro-model, only	0	2.48	65.45	66.54	371.8
2	FE macro/micro-model	0	2.34	59.64	68.1	468.5
3	FE macro model, only	0.28	2.55	65.45	66.54	382.2
4	FE macro/micro-model	0.28	2.41	59.64	68.1	483.9

4. Modelling results

4.1. Contact results

To check the accuracy of the displacement coupling technique introduced, at first, normal contact problems (with contact elements oriented perpendicular to the contact surfaces) for different cases were solved. For each case, the following contact parameters were evaluated:

- Total approach: δ,
- Representative sizes of the contact area (parallel and transverse to the sliding direction) $2a$ and $2b$,
- Contact pressure distribution and its maximum: $p_{\max}$.

4.1.1. P-fibre orientation

The contact parameters are summarized in Table III. In the frictionless cases, the FE macro-model produces practically a circular contact area (Case 1), while under a macro/micro-model approach (Case 2) the contact area is shorter in the fibre relative to the perpendicular direction. The pressure maximum, in Case 2, is greater than in Case 1, representing the more direct influence of the stiffer fibre in the micro-model. The total approach is smaller in the case of macro/micro-models (Cases 2 and 4) than in the cases of macro-models only (Case 1 and 3). The reason is, that the fibers in the micro-models are less deformable than the anisotropic model itself due to the different stiffness parameters. If friction is considered there are no significant differences in the contact parameters (if the corresponding models for the different fibre orientation are compared; see later). The reason is that the friction force, acting in the fibre direction can not increase the bending load of the load carrying fibers. At the same time, stresses in fibre direction are different if friction is considered.

Fig. 3a illustrates the contact pressure distribution. The normal and friction forces are practically transferred by the fibers, due to their higher stiffness.

The contact results for P-fibre orientation do not agree with Ovaert's results [4] in the characteristic shape of the contact area. By the present technique the shape of the contact area is near to circular, while long and narrow, elliptical contact areas were presented in [4].

TABLE II Characterization of the micro-models

Fibre orientation	Size of the micro-model	Number of the solid elements	Number of the contact elements
Parallel (P)	120 μm × 45.75 μm × 45.75 μm	54080	670
Anti-parallel (AP)	90 μm × 60 μm × 45.75 μm	54080	671

TABLE IV Contact parameters for normal and frictional contact problems in the case of AP-fibre orientation

Case no.		μ	δ (μm)	$2a$ (μm)	$2b$ (μm)	p_{max} (MPa)
1	FE macro-model	0	2.48	66.54	65.44	371.9
2	FE macro/micro-model	0	2.34	68.1	59.64	468.5
3	FE macro model	0.3	2.64	66.54	65.44	365.9
4	FE macro/micro-model	0.3	2.48	68.12	65.78	517.6

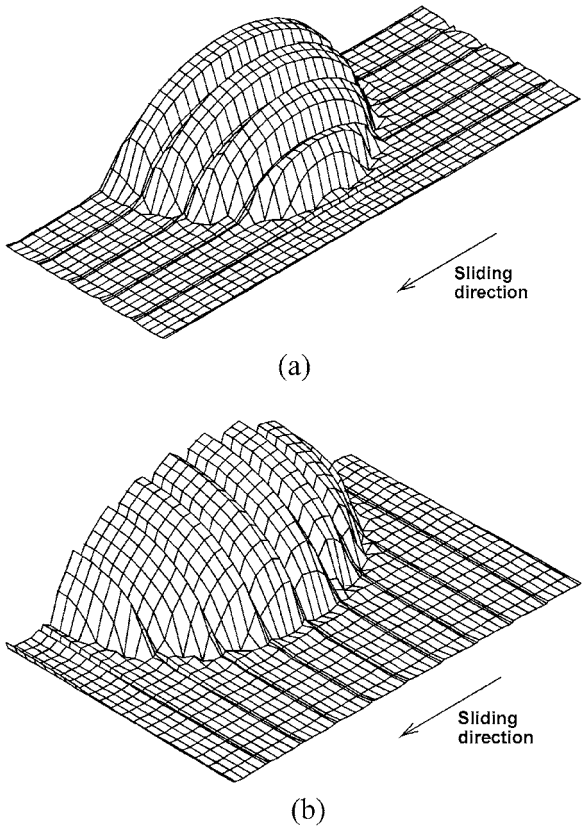

Figure 3 Contact pressure distribution in the case of P-fibre orientation (a) and AP-fibre orientation (b).

4.1.2. AP-fibre orientation

For AP-fibre orientation the frictionless contact results are the same as in the case of P-fibre orientation. If friction is considered, the macro-models produce a slightly different behaviour (see Case 3 in Tables III and IV). The FE macro/micro model can characterize the specific contact behavior of the AP-fibre orientation. In Table IV, the pressure maximum is higher for Case 4 than for Case 2, due to the torsion of the loaded fibers produced by the friction force. This behavior is visible in Fig. 3b if the shape of the pressure peak is studied over the loaded fibers.

The contact results for AP-fibre orientation do not agree in their tendencies with Ovaert's results [5]. In [5] long and narrow, elliptical contact areas were presented, whereas the shape of the contact area is almost circular according to the present technique. It was also verified in [6] by both a numerical contact analysis and experimental techniques.

4.2. Displacement and strain results

4.2.1. P-fibre orientation

The deformed shape of the composite micro-structure, being in contact under P-orientation with the sliding steel asperity, is illustrated in Fig. 4a. The dominant deformation is caused by compression of the composite system and a bending type loading of the fibers.

TABLE V Different strain components in the fibers and the matrix in the case of P-fibre orientation. The bold numbers refer to the most critical normal and shear strain values in the matrix

	Fibers		Matrix	
	Min	Max	Min	Max
ε_x	−0.0068	0.0085	−0.0137	**0.0231**
ε_y	−0.0055	0.0028	−0.0056	0.0027
ε_z	−0.0260	0.0025	−0.0567	0.0070
γ_{xy}	−0.0060	0.0109	−0.0304	0.0326
γ_{xz}	−0.0217	0.0136	−0.0624	0.0208
γ_{yz}	−0.0225	0.0324	−0.0584	**0.1048**
ε_{eq}	0	0.0212	0	0.0638

TABLE VI Different strain components in the fibers and the matrix in the case of AP-fibre orientation. The bold numbers refer to the most critical normal and shear strain values in the matrix

	Fibers		Matrix	
	Min	Max	Min	Max
ε_x	−0.0049	0.0028	−0.0045	0.0024
ε_y	−0.0163	0.0142	−0.0323	**0.0321**
ε_z	−0.0268	0.0067	−0.0592	0.0195
γ_{xy}	−0.0038	0.0191	−0.0144	0.0523
γ_{xz}	−0.0269	0.0040	−0.0838	0.0021
γ_{yz}	−0.0164	0.0304	−0.0388	**0.0906**
ε_{eq}	0	0.0226	0	0.0578

The maximum/minimum values of various strain components are collected in Table V for the fibers as well as the matrix material. Considering the absolute values, the highest one is found for the shear strain γ_{yz} in the matrix (Fig. 4b). It takes place around the mostly loaded surface fibers, at the front side of the contact area, and it is produced by the deformation due to normal and friction forces. According to these results, shear deformation and compression can finally yield to a shear type failure of the matrix material. In addition, the relatively high normal strains in x-direction (ε_x) may cause failure of the fibre/matrix interfacial regions.

4.2.2. AP-fibre orientation

The deformed shape of the composite micro-structure under AP-orientation is shown in Fig. 5a. The dominant deformation is characterized by a compression of the composite system, furthermore by bending and torsion type loading of the fibers.

Table VI summarizes the maximum/minimum values of the different strain components related to the fibers and the matrix material respectively. The highest shear strains are again represented by the γ_{yz}-component of the matrix (Fig. 5b). Its maximum is located around the mostly loaded fibers at the front side of the contact area. Again, one can conclude that shear type failure characterizes the matrix behavior.

4.3. Stress results

4.3.1. P-fibre orientation

Table VII lists the maximum/minimum stress values for the fibers and matrix respectively. The highest stresses

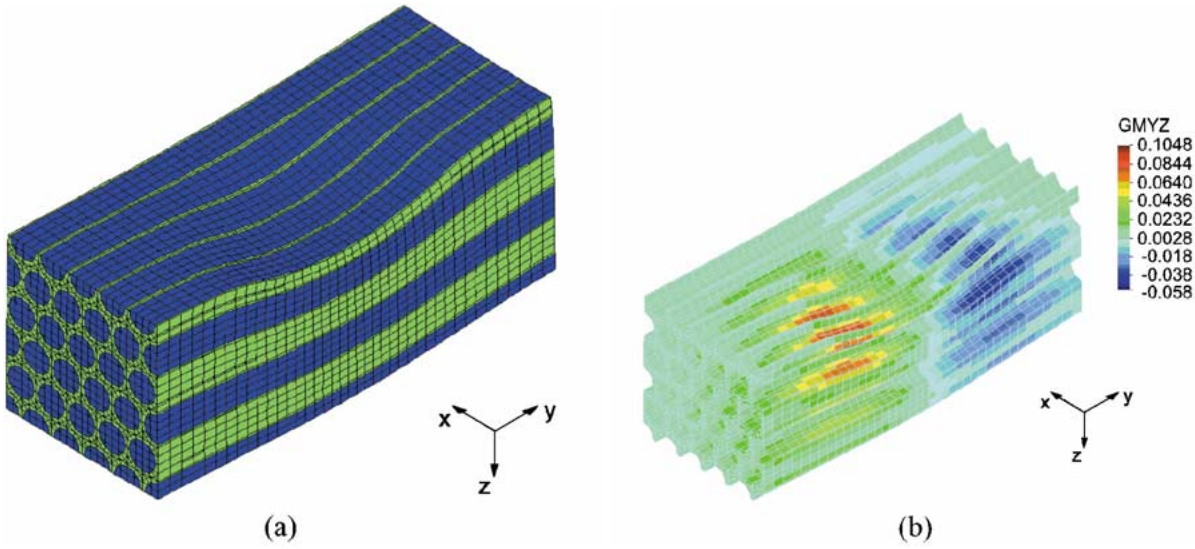

Figure 4 Deformed shape of the "micro-environment" in the case of P-fibre orientation (a) and the γ_{yz} strain component in the matrix in the case of P-fibre orientation (b); (deformation scale 5:1).

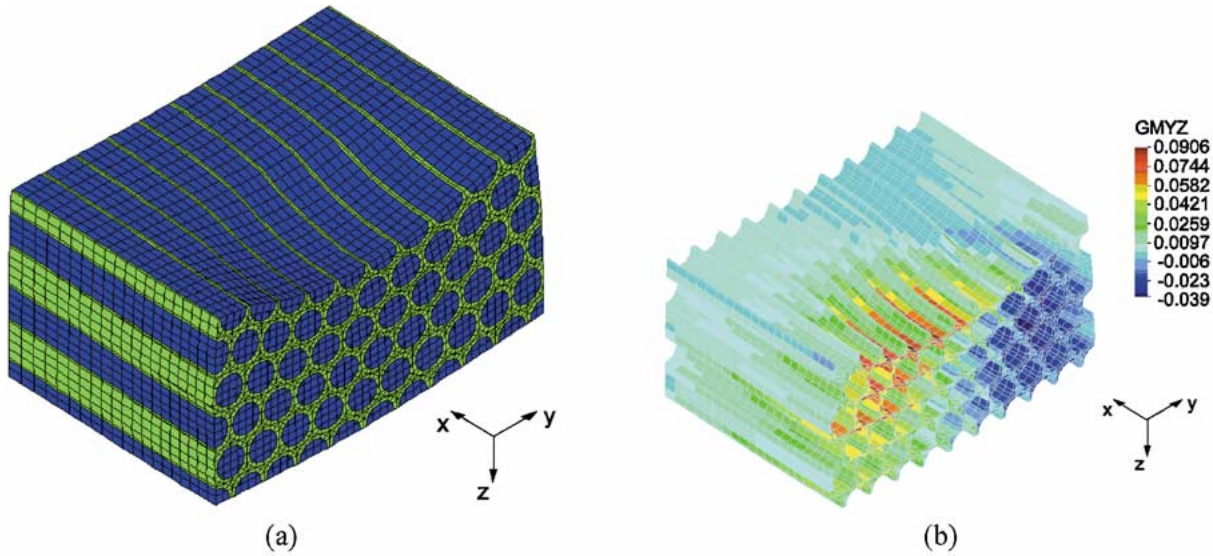

Figure 5 Deformed shape of the "micro-environment" in the case of AP-fibre orientation (a) and the γ_{yz} shear strain component in the matrix in the case of AP-fibre orientation (b); (deformation scale 5:1).

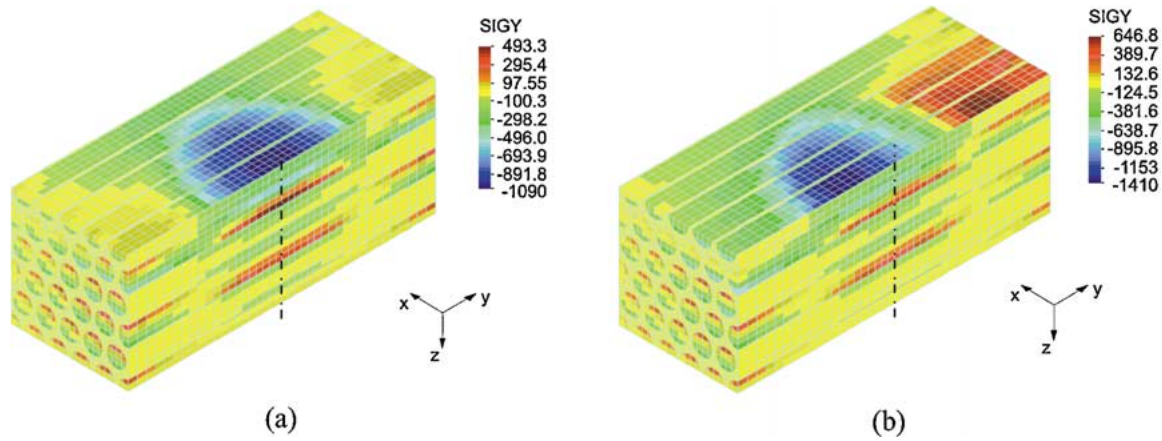

Figure 6 The σ_y stress component (in MPa) in the composite under P-fibre orientation in case of pure compression i.e. without frictional forces (a), and the corresponding stress pattern with an additional friction load (b). The center line indicates the momentary position of the acting counterpart asperity.

occur within the fibers in y direction. These fibers are subjected to bending, transversal compression, and traction within the contact area (see Fig. 4a). This behavior is reflected in rather high values of σ_y in Fig. 6. If no friction is considered (Fig. 6a), bending produces a symmetric stress distribution (without traction) relative to the x-z plane. An additional friction force, however, modifies the stress pattern (Fig. 6b). Behind the contact area, tension appears in the mostly loaded fibers, and the magnitude of the maximum compression stress in

TABLE VII Different stress components in the fibers and matrix in the case of P-fibre orientation

	Fibers		Matrix	
	Min	Max	Min	Max
σ_x(MPa)	−307.18	64.42	−312.49	**60.25**
σ_y(MPa)	−1410.1	646.81	−314.47	21.43
σ_z(MPa)	−483.84	11.28	−451.39	10.80
τ_{xy}(MPa)	−36.39	69.93	−43.72	46.89
τ_{xz}(MPa)	−116.51	72.87	−89.79	29.93
τ_{yz}(MPa)	−144.57	208.13	−84.09	**150.86**
σ_{eq}(MPa)	0	1166.7	0	275.37

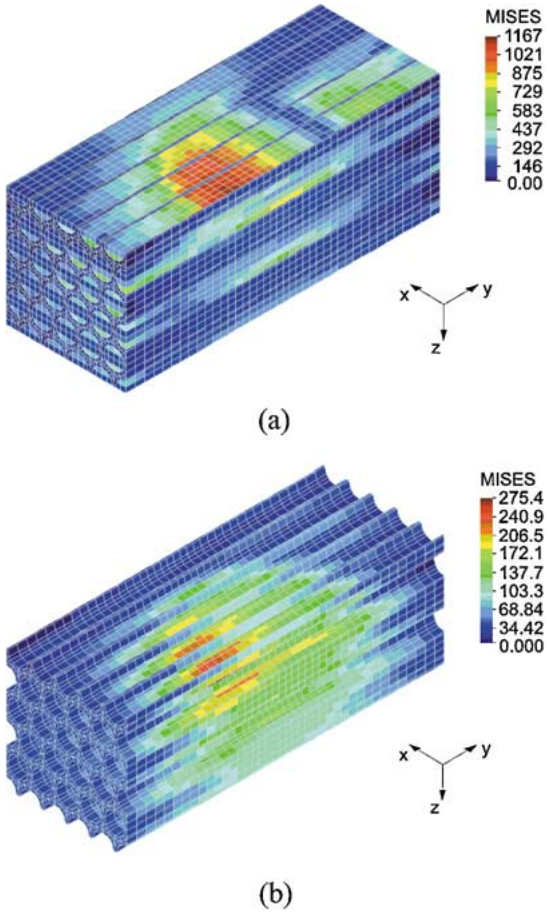

Figure 7 The Mises stress distribution (σ_{eq} in MPa) within the composite in the case of P-fibre orientation (a) and the Mises equivalent stress (σ_{eq}) in the matrix under this fibre orientation (b).

the middle of the contact area is increased. The location of the maximum compression region is moved further to the sliding direction due to the effect of the friction force. The Von Mises type equivalent stress distribution is illustrated in Fig. 7a, showing strong similarities to the distribution of σ_y. The maximum values can eventually exceed the strength of the fibers in the region of highest stress concentration, thus leading to fibre cracking events in the contact surface.

According to Table VII, the most dominant stress component in the matrix is the shear stress τ_{yz}, which, in turn, has lead to the high shear strain γ_{yz}. As a result, local shear failure of the matrix and fibre/matrix debonding phenomena (also due to the high normal stress σ_x) can take place. The highest equivalent stress distribution in the matrix (Fig. 7b) is 275 MPa, is mostly due to the shear stress τ_{yz}, located just below the mostly loaded half-fibers. The approximate extension of the plastic

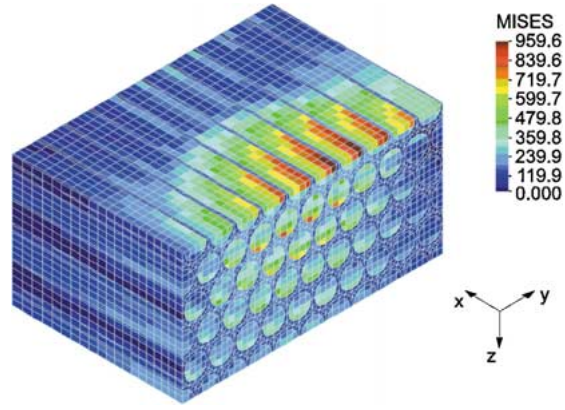

Figure 8 The Mises equivalent stress distribution (σ_{eq} in MPa) in the composite for the case of AP-fibre orientation.

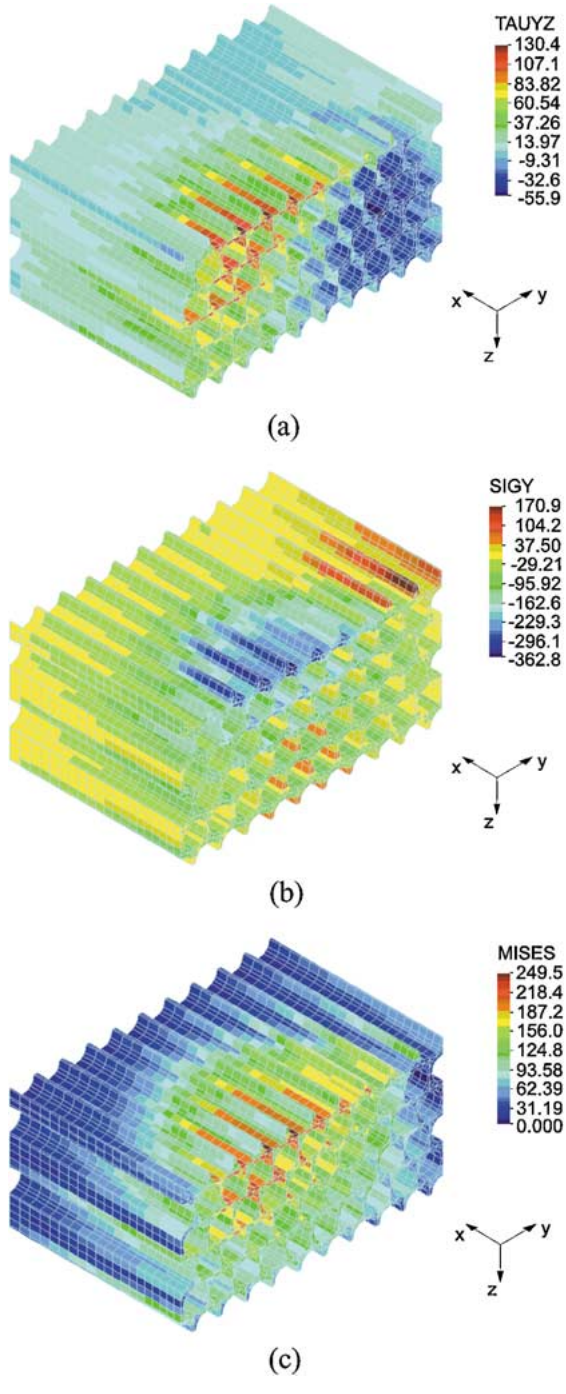

Figure 9 The τ_{yz} stress component (a), the σ_y stress component (b), and the Mises equivalent stress (σ_{eq}) in the matrix (c) for the case of AP-fibre orientation (in MPa).

zone in the matrix is the zone of the highest equivalent stresses, yielding to matrix failure in this narrow vicinity of the contact area in the depth direction. The corresponding depth is about double the fibre diameter.

The other feature of the stresses in the matrix (see Table VII) is a near-to-hydrostatic stress state. The minimum values of σ_x, σ_y and σ_z are about in the same range, producing compression in the local vicinity of the contact area. In this vicinity the "near-to-hydrostatic" stress state will increase the yield strength of the matrix material. This feature should be considered later in the non-linear analysis.

4.3.2. AP-fibre orientation

Table VIII lists the maximum/minimum stress values for the fibers and matrix respectively. The highest stresses within the fibers are found in x direction. This is due to a complex loading situation of the fibers, consisting of transverse compression, bending and torsion. The corresponding equivalent stress distribution in the composite is illustrated in Fig. 8. Due to the compressive stress component in z-direction, the formation of a groove on the composite surface under the influence the sliding asperity is most probable. The bending component acting in y-direction, on the other hand, may lead to fibre cracking phenomena in the center and at the edges of the groove, finally resulting in the removal of broken fibre fragments out of the groove due to the torsion forces acting on them.

According to Table VIII, the most dominant stress component in the matrix is the shear stress τ_{yz}. In addition, the horizontal stress component σ_y has an important effect on the behavior of the matrix (Fig. 9). In the front part of the contact area, high compression arises in y direction (due to the friction force), while behind the contact area tension represents this stress component. Both can contribute to fibre/matrix transverse debonding phenomena due to the cyclic effect during the repeated motion of the asperities. One can conclude that matrix failure due to shear and tension/compression type fibre/matrix debonding may occur in the case of AP-fibre orientation. These effects also characterize the equivalent stress distribution (Fig. 9c). According to the individual results, τ_{yz} has the most dominant effect on the equivalent stresses. From the latter, it can also be concluded that the field of higher stresses reaches below the contact area down to a depth of about the double size of the fibre diameter. This means, also fibre/matrix debonding phenomena may take place underneath the direct contact area of the sliding partners.

TABLE VIII Different stress components in the fibers and matrix in the case of AP-fibre orientation

	Fibers		Matrix	
	Min	Max	Min	Max
σ_x(MPa)	−1281.1	586.45	−341.25	74.63
σ_y(MPa)	−401.02	182.58	−362.77	**170.92**
σ_z(MPa)	−517.62	104.12	−490.53	62.32
τ_{xy}(MPa)	−24.16	123.19	−20.79	75.26
τ_{xz}(MPa)	−172.79	25.73	−120.55	2.97
τ_{yz}(MPa)	−87.70	163.07	−55.87	**130.39**
σ_{eq}(MPa)	0	959.58	0	249.55

5. Experimental verification by scratch tests

5.1. P-fibre orientation

The wear mechanisms under P-fibre orientation are shown in Fig. 10. For better visibility, only the results of the diamond indentor under a load of 3 N are presented. Within the single wear groove in the center part of Fig. 10a, clear features of fibre/matrix debonding, fibre bending and transverse fibre fracture are detectable (see arrows). Right and left from the groove, the polished surface remained in its undamaged state. At a ten times higher magnification (Fig. 10b), a more densely packed crack pattern, with cracks transferring from one fibre to the next, are noticeable. In addition, the formation of shear features which look similar to the practically rolled matrix debris ("rollers") known from mode II (in plane shear)-type interlaminar fatigue fracture surfaces of CF-PEEK-composites [13], can be found. All these findings are in good agreement with the wear mechanisms expected from the FE-predictions. They can also be found for the lower loading cases and the steel ball experiments, although they are not as frequent and clearly detectable as in the present case.

5.2. AP-fibre orientation

Fig. 11 illustrates the failure mechanisms within a wear groove of an AP-fibre oriented composite, as produced under diamond indentor scratching with a load of 3 N. It becomes obvious, that the compressive and frictional loads of the indentor have caused bending of the fibers into the surface and in the sliding direction. Both were associated with fibre fracture events in the center region of the core as well as in the transition between the groove and the undamaged area. Some of the broken fibre segments were removed out of the actual groove area (arrow on Fig. 11a), which could have been a result of the additional torsional moments acting in the scratched material surface. Fig. 11b enlarges a damaged region in the core of the groove, indicating fibre/matrix debonding phenomena (arrow), further fracture of broken fibers into many small fragments (arrow), and again the shear rolled features of the matrix material between the broken fibers (as already described for the P-orientation). Also here, the features observed agree well with the FE-predictions. In addition, the same effects, although to a lower extent, are found for slightly higher loads and a steel ball indentor. An example for the latter is given in Fig. 12 for the P-orientation.

6. Discussion of stress type failure conditions and wear mechanisms

The micro-models presented can evaluate the strain and stress components in a real fibre/matrix "micro-environment" more precisely than can be obtained by a macroscopic approach. Therefore, the present results can be used for further failure analysis and the prediction of wear mechanisms in a much better way.

6.1. P-fibre orientation

For failure analysis and wear prediction, Ovaert [4] evaluated the fibre stresses using an individual fibre model with an elastic foundation. He concluded, that

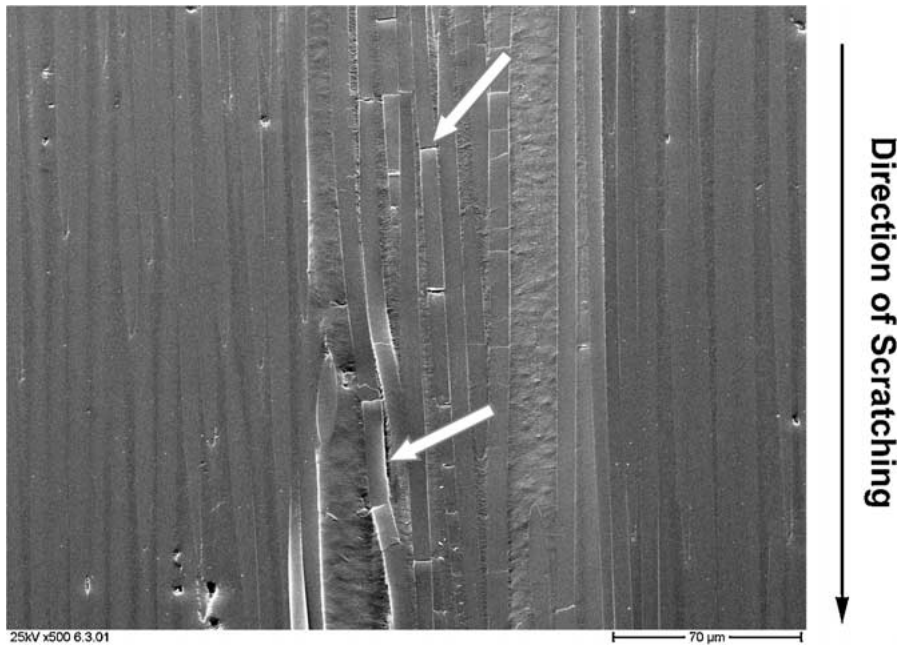

(a)

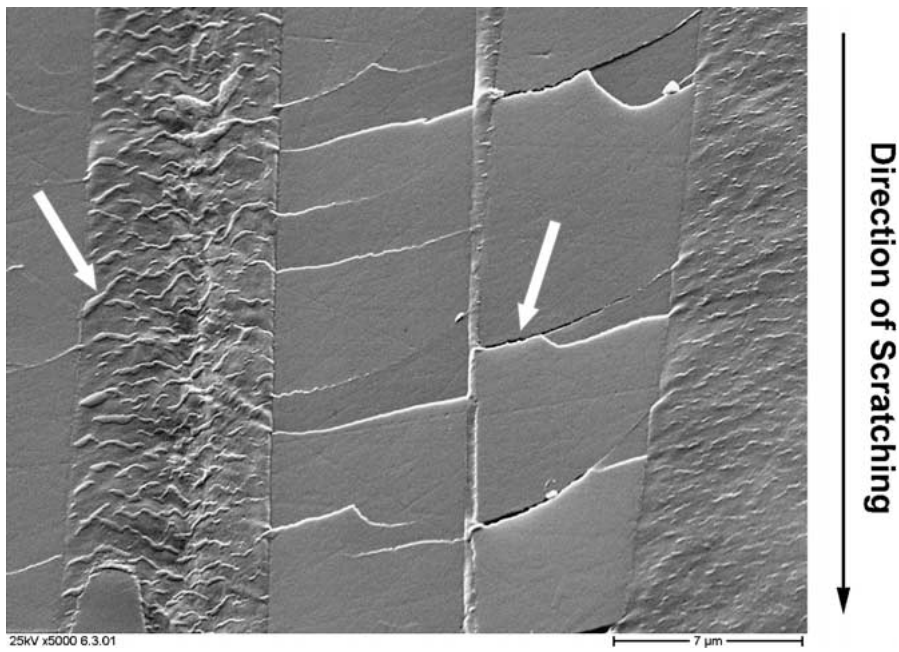

(b)

Figure 10 A single wear groove on a polished P-oriented CF/PEEK-surface, as produced by a diamond indentor under a load of 3 N (a), and details of the failure mechanisms in the center part of the groove (b).

tensile stresses induced in the surface fibers produce fibre breakage and lead to fibre/matrix separation.

According to our results, the combined loading of compression, traction and bending can cause high σ_y stresses, in the fibers so that fibre cracking events are also very likely. In fact, the scratch tests showed also fibre cracking phenomena. Especially in the course of the wear process, after fibre thinning and fibre/matrix delamination, fibre cracking can become an important mechanism.

The matrix material, in a small vicinity of the contact area and especially in depth direction, is also subjected to high stresses. For example, the maximum equivalent stress is above the yield strength of the matrix material (see Table I). As a result, plastic deformation of the matrix under shear loading conditions should occur. In Table V, the highest strain component is γ_{yz} (about 10%), arising in y direction, below the mostly loaded surface fibers. This shear strain can also produce shear type fibre/matrix debonding if the shear stresses are above the debonding strength of the CF/PEEK material [8]. During the repeated sliding motion this debonding can propagate to the surface, producing a complete debonding of the surface fibers. Based on various measurements, the shear type debonding strength of CF/PEEK is of the order of about 60 MPa, i.e. significantly below the actual maximum shear stress values. It can, therefore, be concluded, that shear type debonding is a dominant failure mechanism in the case of P-fibre orientation, representing the starting phase of the wear process. This debonding can produce a different, partly separated micro-structure, that has less wear

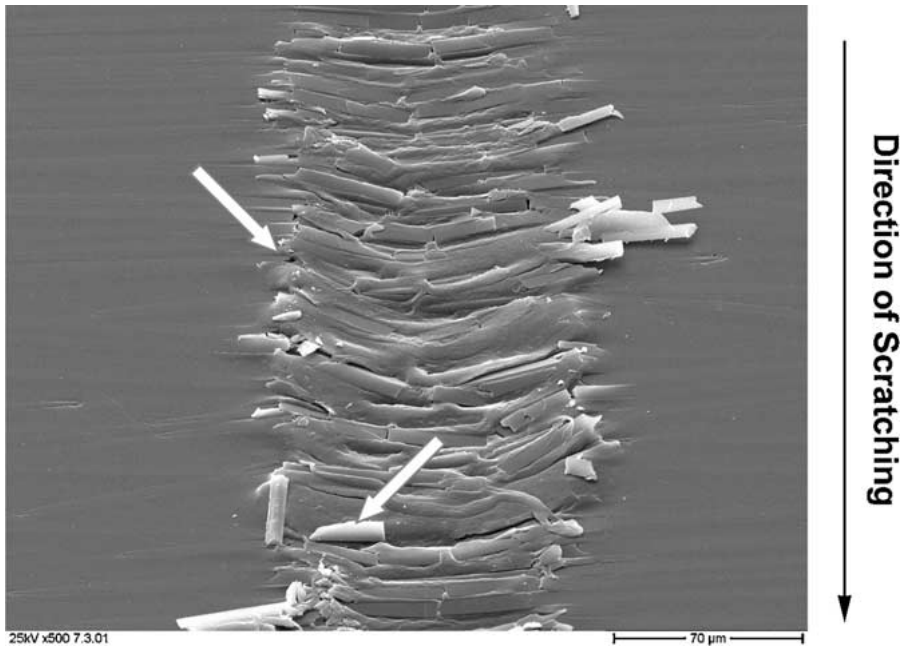

(a)

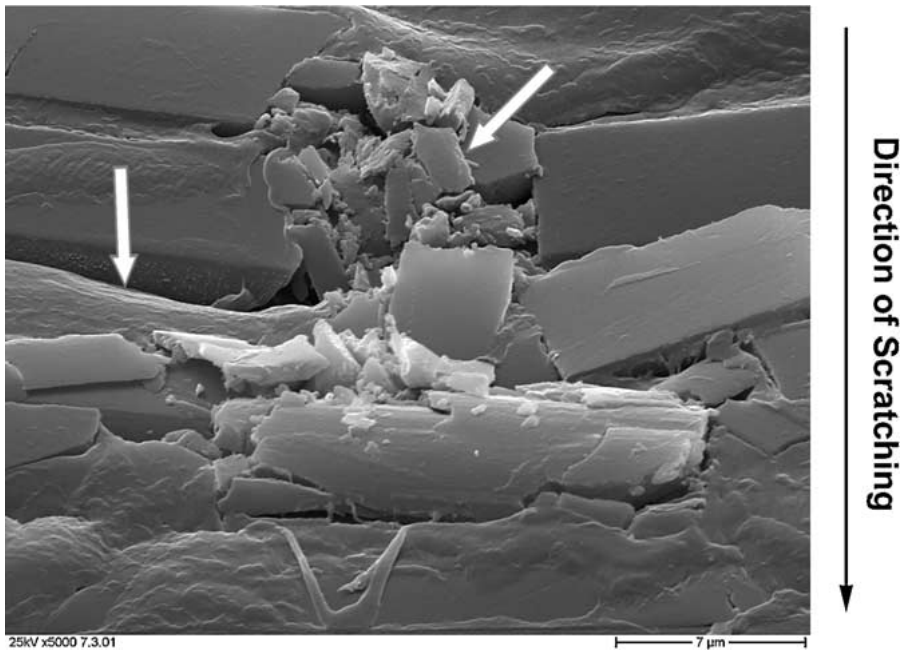

(b)

Figure 11 A single wear groove on a polished AP-oriented CF/PEEK-surface, as produced by a diamond indentor under a load of 3 N (a), and details of the failure mechanisms in the center part of the groove (b).

resistance than the original one, due to higher, more critical stresses. This debonding was observed in Fig. 10a.

6.2. AP-fibre orientation

Referring to Ovaert's works [5], the non-dimensional stress-deformation parameter introduced gives values for the AP-fibre orientation, which are 2–5 times higher than for the P-fibre orientation, due to the elliptical shape of the contact area (usually with an axis ratio of 1 : 7). If a near-to-circular contact area is considered, as observed in our results, the stress-deformation parameters for both fibre orientation are much closer to each other, yielding to less different wear rates for the P- and AP-fibre orientation. In fact, the latter was observed in our previous experimental results [14], although the figures in this paper (Fig. 10a vs. Fig. 11a) give the impression that the AP-orientation results in much higher wear rates.

Considering the mostly loaded surface fibers, at first, the high σ_x stresses (Table VIII) are caused by compression, traction and bending. As a result, fibre cracking and fibre fragment removal can take place, as observed in the real scratch tests. But this is true mainly for the higher loads, which probably do not represent the actual case in the real sliding experiments.

The matrix material, in depth direction, within a small vicinity of the contact area, is also subjected to high stresses (Table VIII). The maximum equivalent stress is above the yield strength of the matrix material so that the observed shear type deformation is not surprising. In Table VI, the highest strain γ_{yz} is about 9%, and the second highest one γ_{xz} is greater than 8%. Both

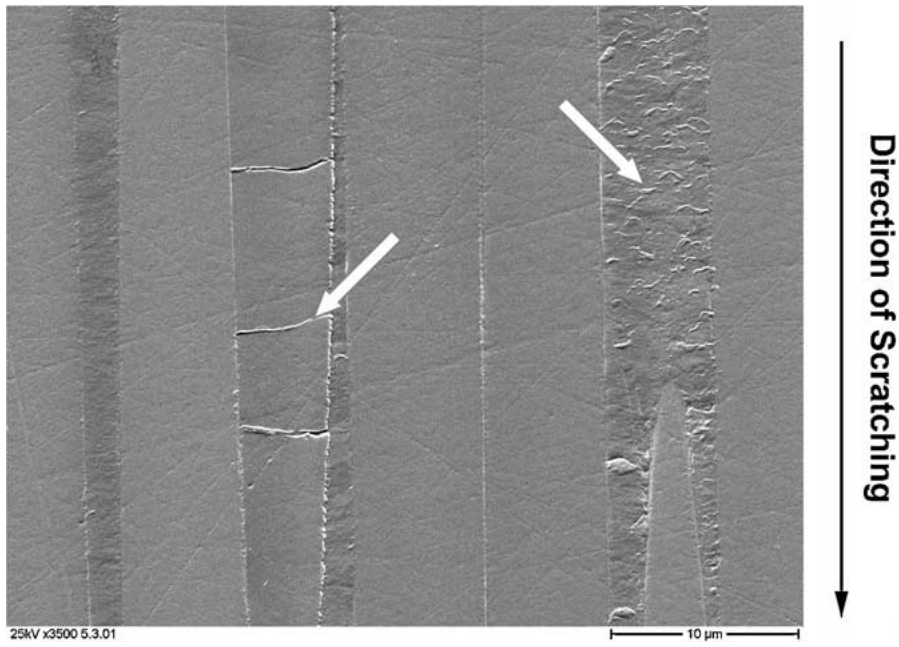

Figure 12 Local damage of fibers (cracks: see left arrow) and shear features of the matrix (rollers: see right arrow) within a single scratch on a polished P-oriented CF/PEEK-surface. The scratch was produced by a 0.9 mm diameter steel ball under a load of 5 N.

of them are located below the mostly loaded surface fibers, where they can produce shear type debonding if the shear stresses exceed the debonding strength of the CF/PEEK material. Furthermore the high σ_y stress can cause tension/compression type debonding there. During the repeated sliding motion this debonding can propagate to the surface, producing a complete debonding of the surface fibers.

One can conclude, that the shear and tension/compression type debonding is also one of the dominant failure mechanisms in the case of AP-fibre orientation, representing the starting phase of the wear process.

Comparing the results obtained by the FE contact micro-models for P- and AP-fibre orientations, it can be concluded that in the case of the sliding asperity studied the AP-fibre orientation produces lower fibre stresses (by about 15%) and lower matrix stresses (by about 10%). This would imply a lower probability for wear failure under AP in comparison to P-fibre orientation. This is opposite to the impression one has from the scratch experiments. One therefore must conclude, that the prediction of less failure can not generally be forecast for the sliding contact of real composite steel surfaces because neither wear debris nor transfer film layer effects were considered in the model. Under real sliding conditions, in the case of AP-fibre orientation, the wear debris (formed from broken fibre peaces) has probably a more dominant effect on the wear process than in the case of P-fibre orientation. Considering these conditions will require more complex simulation models.

7. Conclusions

(a) By modelling the fibre/matrix micro-structure, the FE macro/micro contact model developed (introducing the displacement coupling technique), is much more suitable for studying failure mechanisms in real fibre-reinforced composites vs. steel than using an equivalent macro-model, therefore the calculated contact, stress and strain results are significantly closer to real conditions.

(b) Based on the FE micro-models, possible failure mechanisms of the fibre-reinforced composite have been explored. For P-fibre orientation, the fibre/matrix debonding by shear type deformation and fibre sliding wear are the dominant failure mechanisms. If AP-fibre orientation is considered, the shear and the tension/compression type debonding are the most dominant wear mechanisms.

(c) As regards the failure of the fibre/matrix interface, in the case of each fibre orientation local debonding is probably the starting step of the wear process. If a partly debonded micro structure is subjected to a repeating sliding asperity, the stresses will be higher producing more critical failure in the near region of the contact area.

(d) According to the experimental verification, prepared by the scratch test, abrasive and adhesive matrix failure furthermore fibre/matrix debonding were observed on SEM photos.

(e) Based on these findings, a better composite design/manufacturing e.g., providing stronger bonding and material selection can reduce the predicted fibre/matrix debonding. A stronger bonding can also increase the wear resistant of the composite material.

(f) Studying these phenomena on a more accurate level requires models, locating contact elements between the debonded surfaces. Due to the high stress values in the matrix, a non-linear analysis would be more appropriate to follow both the plastic behavior of the matrix and the shear failure at the fibre/matrix interface. Our intention is to create these models in the near future.

Acknowledgements

The presented research was first of all supported by the Deutsche Forschungsgemeinschaft (DFG FR675/19-2). Additional help by the Hungarian National

Scientific Research Foundation (T 023351) and by the BMBF-TéT as part of the German-Hungarian research co-operation on contact mechanics of different materials is also gratefully esteemed.

Appendix

Anisotropic material properties for the composites (considering anisotropic fibre) [3].

$$
\begin{aligned}
E_{11} &= E_{f11}V_f + E_m V_m, \\
\frac{1}{E_{22}} &= \frac{V_f}{E_{f22}} + \frac{V_m}{E_m}, \\
E_{33} &= E_{22}, \\
v_{12} &= v_{f12}V_f + v_m V_m, \\
v_{13} &= v_{12}, \\
v_{23} &= v_{f23}V_f + v_m V_m C \\
C &= \frac{1 + v_m - v_{21}\frac{E_m}{E_{11}}}{1 - v_m^2 + v_m v_{21}\frac{E_m}{E_{11}}}, \\
\frac{v_{12}}{E_{11}} &= \frac{v_{21}}{E_{22}}, \\
\frac{1}{G_{12}} &= \frac{V_f}{G_{f12}} + \frac{V_m}{G_m}, \\
G_{13} &= G_{12}, \\
G_{23} &= \frac{E_{33}}{2(1 + v_{23})}.
\end{aligned}
$$

References

1. K. FRIEDRICH, COMETT-Workshop on "Tribology of Materials," (Lausanne, Switzerland, September 1993).
2. H. VOSS, and K. FRIEDRICH, *Wear* **116** (1987) 1.
3. K. K. CHAWLA, "Composite Materials" (Springer-Verlag, New York, 1987).
4. T. C. OVAERT, *Tribology Transactions* **38**(1) (1995) 27.
5. *Idem.*, *Tribology Transactions* **40**(2) (1997) 227.
6. K. VÁRADI, Z. NÉDER, K. FRIEDRICH and J. FLÖCK, *Composites Science And Technology* **59** (1999) 271.
7. COSMOS/M User Guide, V2.0, Structural Research and Analysis Corporation (1998).
8. XC-2 Wear Resistant Composites, ICI Thermoplastic Composites (1993).
9. VDI Wärmeatlas, 3. Auflage (1997).
10. F. N. COGSWELL, "Thermoplastic Aromatic Polymer Composites" (Butterworth-Heinemann Ltd., Oxford, 1992).
11. J. FLÖCK, K. FRIEDRICH, *Experimentelle Untersuchungen zur Transferfilmbildung kontinuierlich kohlenstoff-faserverstärker Polyetheretherketon (PEEK) Verbundwerkstoffe auf einem 100Cr6 Stahlring*, Gft Tribologie-Fachtagung, Göttingen, 28. bis 30. September, Bound 1, Vortrag Nr. 9 (1998) p. 1.
12. T. GODA, K. VÁRADI, K. FRIEDRICH and H. GIERTZSCH, *J. Mater. Sci*. **37** (2002) 1575.
13. K. FRIEDRICH, "Application of Fracture Mechanics to Composite Materials," edited by K. Friedrich, Composite Materials Series no. 6, Series Editor: R. B. Pipes (Elsevier, Amsterdam, The Netherlands, 1989) ch. 11, p. 425.
14. J. FLÖCK, in "IVW Schriftenreihe Band," edited by M. Neitzel Vol. 19 (Kaiserslautern, Germany, 2001). ISBN 3-934930-19-0.

Received 4 June 2001
and accepted 10 April 2002